Vietnam Journal of Science and Technology ***56*** *(2A) (2018) 217-225*

NUMERICAL SIMULATION OF ELECTROCHEMICAL CHANGES IN THE STUDY OF CORROSION IN AN OCCLUDED ZONE

Vu Anh Quang[1, *], Luu Hoang Tam[1], Nguyen Nhi Tru[1], Vinh-Dat Vuong[1, 2, 3], Le Van Thang[1, 2]

[1]*Department of Energy Materials, Faculty of Materials Technology, HCMUT–VNUHCM*
268 Ly Thuong Kiet Street, Ward 14, District 10, Ho Chi Minh City, Viet Nam

[2]*Materials Technology Laboratory, HCMUT–VNUHCM*
268 Ly Thuong Kiet Street, Ward 14, District 10, Ho Chi Minh City, Viet Nam

[3]*Graduate University of Science and Technology, VAST*
18 Hoang Quoc Viet Streem Cau Giay District, Ha Noi City, Viet Nam

[*]Email*: vaquang@hcmut.edu.vn*

Received: 12 March 2018; Accepted for publication: 13 May 2018

ABSTRACT

An experimental setup allowing pH measurements inside a confined volume representing a lapped joint was designed in our last study [1]. The pH evolution over steel surface in confined conditions was monitored. In this study, the experimental pH was compared with that calculated using a two-dimensional transport-reaction model only in the case of a confined iron surface. The difference between the experimental and calculated pH in the steady state was attributed to the limitation of the modelling approach, more especially concerning solid phases precipitation inside the cavity. Nevertheless, only short term (hour) experiments and simulations can be compared illustrating the necessary improvement of these basic models to predict real perforation corrosion rate at long term.

Keywords: galvanized steel, lapped joint, pH measurement, numerical simulation.

1. INTRODUCTION

In Viet Nam, some scientists have recently started using COMSOL Multiphysics software in their research. However, the number of studies and research areas is limited. In 2012, a COMSOL Multiphysics software application in intelligent inkjet nozzle simulation was performed by Hoang Cuong [2]. In 2014, Le Minh Thanh [3] and colleagues simulated a decrease in dissolved oxygen concentration by the lake depth by this software. According to our knowledge, no study has been published using COMSOL Multiphysics software for numerical simulation of electrochemical corrosion in an occluded zone. Most recently, the Faculty of Electronics and Telecommunications of Vinh University has a scientific seminar on the design of capacitive sensor design using this software in August 2016. It can be said that the use of this software is still quite new in the scientific research in Viet Nam.

In comparison with Viet Nam, the application of COMSOL Multiphysics software in the world is more popular and in many different fields. Particularly on electrochemical analysis, there are many research applications of this software. A. Ebrahimi Khabbazi [4] studied the effect of the geometry of the electrode. Zhanyu Sun [5] investigated the effect of limited surface conditions on convection and diffusion. Francisco et al. [6] simulated rotary electrodes. Matteo Scaramuzza [7] constructed a model of contact between electrode and electrolyte solution. Eligio P. Rivero [8] simulated mass transfer and predicts mass transfer coefficients using this software. Recognizing the growing demand for COMSOL Multiphysics in electrochemical research, Edmund J.F. Dickinson et al. [9] reported a brief synthesis of using this software in electrochemical analysis. The references of this article showed a wide use of COMSOL Multiphysics software in the field of electrochemistry. Most recently, there have been models for the formation of electrochemical coatings as in the studies of Piyushkumar B. Tailor and Abishek Kamaraj [10, 11]. However, there have been no studies on corrosion in occluded zone.

The pH evolution over steel surface in confined conditions was monitored in our last study [1]. The experimental setup for this type of survey is very hard to control. Moreover, the question is how to have a sufficient and reliable miniature sensor for this measurement in an occluded zone. Thus, under current conditions, we think that the implementation of numerical simulations will allow the computation of chemical and electrical variations in this occluded zone using the finite element method in COMSOL Multiphysics software. In the work described in this paper, the objective of these simulations is not only to validate the experimental results obtained in our last study, but also to predict the evolution of pH in occluded zone for other studies that it is experimentally difficult to achieve the pH measurement.

2. BACKGROUND ON SIMULATION OF MASS TRANSFER CONTROLLED CORROSION PROCESSES USING A FINITE ELEMENT ANALYSIS

The implementation of the 2D model representing the behavior of a cavity formed on the surface of a steel plate (covered or not by a Zn containing coating) is based on models developed successively starting from basic mass transport and reaction 1D models of general corrosion but do not include the effects of precipitation.

In the mass transport and reaction model, the concentration of each species *i*, and the potential distributions were obtained by solving the Nernst-Planck equation in two dimensions (2D) in absence of advection:

$$R_i + D_i \nabla^2 C_i + z_i \frac{D_i}{RT} F \nabla (C_i \nabla \Phi) = \frac{\partial C_i}{\partial t} \tag{1}$$

where R_i is a source term related to the rate of homogeneous chemical reactions, D_i is the diffusivity, C_i the concentration, z_i the charge of species *i*, F the Faraday's constant, R the gas constant and T the temperature.

The electroneutrality condition:

$$\sum_i z_i C_i = 0 \tag{2}$$

is applied to calculate the sodium ion concentration. In this paper, chemical species considered in the models are the following: Na^+, Cl^-, Fe^{2+}, $FeOH^+$, $Fe(OH)_2$, H^+, OH^-, O_2. The 2D-geometry which is implemented for all the models is shown in Figure 1 with the corresponding meshing. The right side of the cell corresponds to the 1 mm or 10 mm length reservoir (mouth), the left

side represents the confined volume. The length of the confined zone varied from 1 mm to 30 mm, to study the effect of the size ratio between the mouth and the confined volume on the current distribution. The boundaries delimiting the subdomain are numbered in Figure 1:

Boundaries 1, 3, 5 and 7 are considered as insulators (zero fluxes at these boundaries): these boundaries correspond to the cavity former (PMMA) and the o-ring in our last study.

Boundary 6 is also supposed to be electrically insulated. This boundary corresponds to the top of the diffusion layer, where the bulk concentrations are imposed for all chemical species.

Boundaries 2 and 4 are the steel surfaces. The electrochemical reactions occurring on the metal surface, with their respective rate law, are the following:

$$Fe \rightarrow Fe^{2+} + 2e^{-}, \qquad j_{Fe} = 2.F.k_{Fe}.\exp\left(\frac{Vm - \Phi - E^{\circ}_{Fe}}{a_{Fe}}\right) \tag{3}$$

$$2H_2O + O_2 + 4e^{-} \rightarrow 4OH^{-}, \quad j_{O_2} = -4.F.k_{O_2}.c_{O_2}.\exp\left(\frac{E^{\circ}_{O_2} + \Phi - Vm}{b_{O_2}}\right) \tag{4}$$

$$2H_2O + 2e^{-} \rightarrow H_2 + 2OH^{-}, \qquad j_{H_2O} = -F.k_{H_2O}.\exp\left(\frac{E^{0}_{H_2O} + \Phi - Vm}{b_{H_2O}}\right) \tag{5}$$

with V_m the metal potential, a_{Fe}, b_{O_2} and b_{H_2O} the Tafel coefficients. For a mixed potential model, a zero current inflow must be imposed all over the metal surface, then: $j_{Fe} + j_{O_2} + j_{H_2O} = 0$. The fluxes of Fe^{2+}, OH^- and O_2 on the metal surface are the following:

$$N_{Fe} = \frac{j_{Fe}}{2F}, \quad N_{OH^-} = -\frac{j_{O_2} + j_{H_2O}}{F}, \quad N_{O_2} = \frac{j_{O_2}}{4F}$$

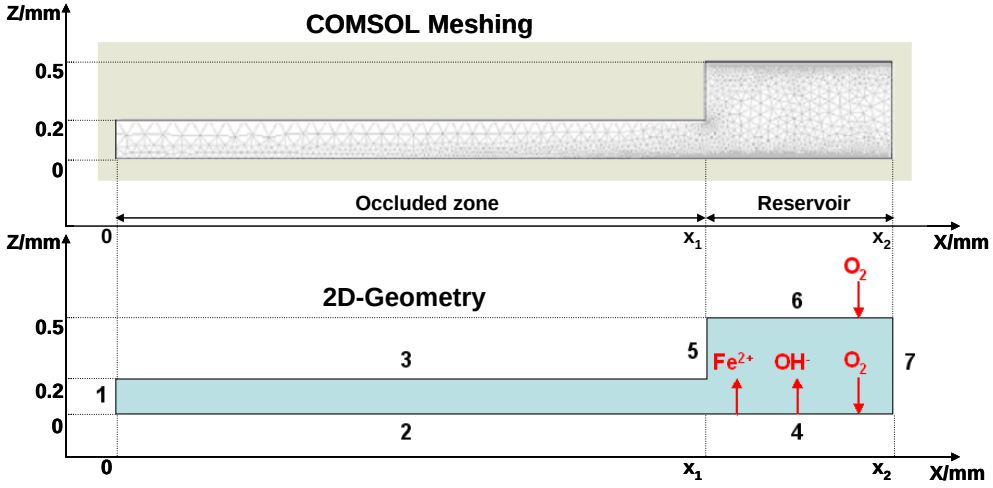

Figure 1. 2D-geometry of the models (with 7 boundaries) with the meshing: the length of the confined volume is given by x1, with x1 = 1, 3, 7, 15 or 30 mm; its height is 0.2 mm; the length of the external bulk solution (reservoir) is given by (x2 – x1), with (x2 – x1) = 1 or 10 mm; its height is 0.5 mm. Boundaries 1, 3, 5 and 7: insulators. Boundary 6: diffusion layer. Boundaries 2 and 4: sample surface.

The following chemical reactions were considered in the solution (subdomain) with their respective law:

$$H_2O \underset{k_{w\_b}}{\overset{k_{w\_f}}{\rightleftharpoons}} H^+ + OH^- \quad (6), \qquad R_w = k_{w\_f} - k_{w\_b}.c_H.c_{OH}$$

$$Fe^{2+} + H_2O \underset{k_{Fe\_b}}{\overset{k_{Fe\_f}}{\rightleftharpoons}} FeOH^+ + H^+ \quad (7), \qquad R_{Fe} = k_{Fe\_f}.c_{Fe} - k_{Fe\_b}.c_{FeOH}.c_H$$

$$Fe^{2+} + 2OH^- \underset{k_{prec\_b}}{\overset{k_{prec\_f}}{\rightleftharpoons}} Fe(OH)_2 \quad (8), \qquad R_{prec} = k_{prec\_f}(c_{Fe}.c_{OH}^2 - K_s)$$

The latter expression for $Fe(OH)_2$ precipitation rate holds only in supersaturated conditions, with a backward precipitation rate equal to $k_{prec\_f}.K_s$.

The expressions for the source term *R* are the following for each species:

Na^+: R = 0

Cl^-: R = 0

Fe^{2+}: R = $-R_{Fe} - R_{prec}$

$FeOH^+$: R = R_{Fe}

$Fe(OH)_2$: R = R_{prec}

H^+: R = $R_w + R_{Fe}$

OH^-: R = $R_w - 2R_{prec}$

O_2: R = 0

Table 1 shows the constants and parameters used for the modelling.

Table 1. Constants and parameters used in the models.

a_{Fe}	0.154	anodic Tafel parameter for iron oxidation (V vs SCE) [12]
b_{O_2}	0.05	cathodic Tafel parameter of oxygen (V vs SCE) [13]
b_{H_2O}	0.05	cathodic Tafel parameter of water (V/SCE) (supposed)
c_{Cl}^0	100	bulk concentration of Cl^- ($mol.m^{-3}$)
c_{Fe}^0	$1.00.10^{-3}$	bulk concentration of Fe^2 ($mol.m^{-3}$)
c_{FeOH}^0	$c_{Fe}^0.K_{Fe}/c_H^0$	bulk concentration of $FeOH^+$ ($mol.m^{-3}$)
$c_{Fe(OH)_2}^0$	0	bulk concentration of $Fe(OH)_2$ ($mol.m^{-3}$)
c_H^0	1.10^{-4}	bulk concentration of H^+ ($mol.m^{-3}$)
c_{Na}^0	100	bulk concentration of Na^+ ($mol.m^{-3}$)
$c_{O_2}^0$	0.26	bulk concentration of oxygen ($mol.m^{-3}$) [14]
c_{OH}^0	K_w/c_H^0	bulk concentration of OH^- ($mol.m^{-3}$)
D_{Cl}	$2.00.10^{-9}$	diffusion coefficient of Cl^- ($m^2.s^{-1}$) [15]

D_{Fe}	$1.00.10^{-9}$	diffusion coefficient of Fe^{2+} ($m^2.s^{-1}$) [15]
D_{FeOH}	$1.00.10^{-9}$	diffusion coefficient of $FeOH^+$ ($m^2.s^{-1}$) [15]
$D_{Fe(OH)_2}$	0	diffusion coefficient of $Fe(OH)_2$ ($m^2.s^{-1}$)
D_H	$9.30.10^{-9}$	diffusion coefficient of H^+ ($m^2.s^{-1}$) [15]
D_{Na}	$1.30.10^{-9}$	diffusion coefficient of Na^+ ($m^2.s^{-1}$) [15]
D_{O_2}	$2.40.10^{-9}$	diffusion coefficient of O_2 ($m^2.s^{-1}$) [15]
D_{OH}	$5.30.10^{-9}$	diffusion coefficient of OH^- ($m^2.s^{-1}$) [15]
E^0_{Fe}	-0.65	standard potential of Fe^{2+}/Fe (V vs SCE) [15]
$E^0_{O_2}$	0.16	standard potential of O_2/OH^- (V vs SCE) [15]
$E^0_{H_2O}$	-1.07	standard potential of H_2O/OH^- (V vs SCE) [15]
F	96485	Faraday constant ($C.mol^{-1}$)
k_{Fe}	$1.45.10^{-6}$	rate constant for iron oxidation ($mol.m^{-2}.s^{-1}$) [12]
k_{Fe_b}	k_{Fe_f} / K_{Fe}	backward kinetics constant for Fe^{2+} hydrolysis ($m^3.mol^{-1}.s^{-1}$)
k_{Fe_f}	$1.00.10^{-3}$	forward kinetics constant for Fe^{2+} hydrolysis (s^{-1})
k_{H_2O}	$1.00.10^{-5}$	rate constant for water reduction ($mol.m^{-2}.s^{-1}$) (supposed)
k_{O_2}	$1.00.10^{-5}$	rate constant for oxygen reduction ($m.s^{-1}$) [16]
k_{prec_f}	100	forward kinetic parameter of $Fe(OH)_2$ ($m^6.mol^{-2}.s^{-1}$)
k_{w_b}	k_{w_f} / K_w	backward kinetics constant for water autoprotolysis ($m^3.mol^{-1}.s^{-1}$)
k_{w_f}	1000	forward kinetics constant for water autoprotolysis ($mol.m^{-3}.s^{-1}$)
K_{Fe}	$10^{-6.5}$	hydrolysis constant of Fe^{2+} ($mol.m^{-3}$)
K_s	$10^{-6.15}$	solubility product of $Fe(OH)_2$ ($mol^3.m^{-9}$)
K_w	$1.00.10^{-8}$	autoprotolysis constant for water ($mol^2.m^{-6}$)
R	8.31	gas constant ($J.K^{-1}.mol^{-1}$)
T	298	temperature (K)
V_m		potential of the metal (V vs SCE)

3. RESULTS AND DISCUSSION

In this paper, a series of models was defined considering a metal surface partially confined as shown in Figure 1. The length of the cavity varies from 1 to 30 mm, and that of the reservoir was 1 or 10 mm. The equality between anodic and cathodic current was systematically checked, with a $(i_{anodic} + i_{cathodic}) < 10^{-9}$ A/m.

The ratios between the steady state cathodic and anodic current integrated over the reservoir and over the confined surface ($\left|i_{H_2O} + i_{O_2}\right| / i_{Fe}$) are given in Table 2 for different lengths of confined volume. It can be seen that whatever the surface area ratio between the

reservoir and the confined volume, the reservoir is mainly cathodic ($i_{cathodic}/i_{anodic} > 1$), whereas the metallic surface in the lapped joint is anodic. The anodic behaviour of the metallic surface in the lapped joint is more pronounced for larger reservoir to confined zone area ratios, i.e. for a cavity length of 3 mm.

Table 2. Ratio between the steady state cathodic and anodic current integrated over the reservoir and the confined surface for different lengths of confined zone (reservoir length = 1 mm).

	Reservoir	Confined zone
Confined zone = 3 mm	3.5	0.2
Confined zone = 7 mm	5.2	0.4
Confined zone = 15 mm	6.1	0.6
Confined zone = 30 mm	6.3	0.8

Table 3 shows the ratios between the steady state cathodic current for oxygen and water reduction integrated over the reservoir and over the confined surface, i.e. i_{O_2}/i_{H_2O}. As expected, oxygen reduction is the main cathodic contribution at the mouth, whereas only water reduction occurs inside the cavity.

Table 3. Ratio between the steady state cathodic current for oxygen and water reduction integrated over the reservoir and the confined surface for different lengths of confined zone (reservoir length = 1 mm).

i_{O_2}/i_{H_2O}	Reservoir	Confined zone
Confined zone = 3 mm	60.7	5.1×10^{-9}
Confined zone = 7 mm	19.4	9.8×10^{-15}
Confined zone = 15 mm	12.9	2.6×10^{-17}
Confined zone = 30 mm	11.6	5.1×10^{-18}

The distribution of the current density in unsteady state conditions for iron oxidation and oxygen reduction are presented respectively in Figure 2 and Figure 3 for a cell geometry similar to that used experimentally, i.e. 10 mm length for the reservoir and 30 mm length for the cavity. In regard of experimental results, the current profiles calculated for the first seconds are meaningless, because they correspond to the time necessary for the setting up of a steady state diffusion current (limited by oxygen reduction) in the reservoir. It can be seen that the anodic current density decreases faster in the cavity than in the reservoir. At long times the anodic current density is slightly lower in the cavity than in the reservoir. This is the reason why the integrated anodic current density (i.e. the anodic current) is higher in the cavity than in the reservoir, leading to a ratio $i_{cathodic}/i_{anodic} = 0.8$ (see Table 2). From numerical simulations it is difficult to determine a time for complete oxygen depletion in the cavity (see Figure 3).

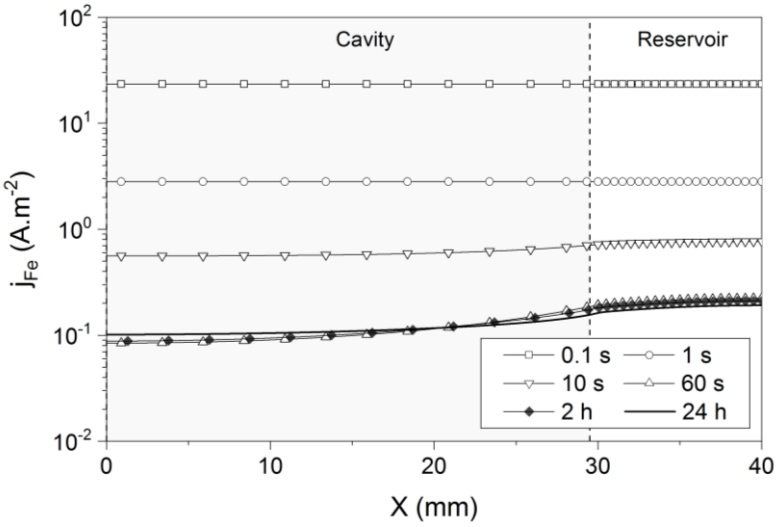

Figure 2. Distribution of the current density in unsteady state conditions for iron oxidation.

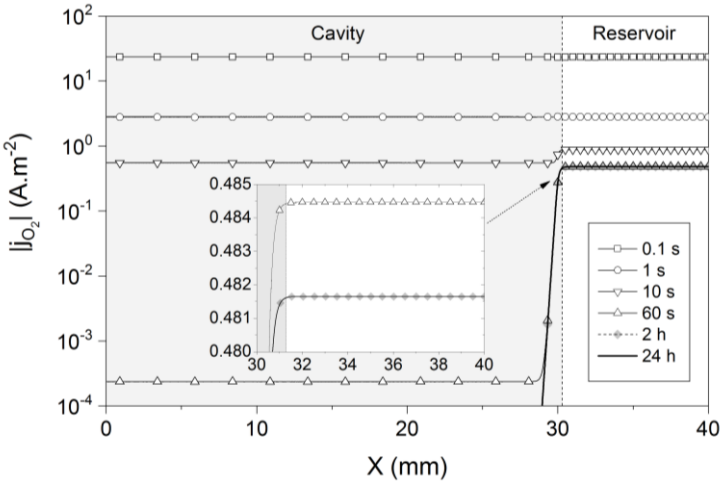

Figure 3. Distribution of the current density in unsteady state conditions for oxygen reduction.

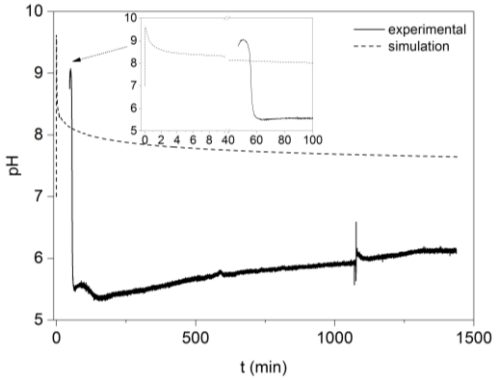

Figure 4. Experimental and simulated pH profiles obtained in the cavity 1 cm far from the mouth and at 200 µm from the steel surface.

Figure 4 superimposed the experimental and simulated pH profiles 1 cm far from the mouth of the cavity, and at a distance of 200 µm from the steel surface. The time shift between basic pH peaks at short times must not be considered because it results most probably from experimental difficulty to get rapidly a confined cell with a given cavity thickness. It appears that acidification of the cavity is faster in the experiment than that simulated. Moreover, the experimental pH obtained in the steady state is about 6, whereas calculation predicts a higher pH value at long times (pH = 7.8). This difference could be lowered, with a more acidic pH obtained by simulation, by considering the presence of CO_2 in the solution. Effectively, the pH of the NaCl solution used for the experience was increased from about 5.6, due to CO_2 dissolution, to pH = 7 with sodium hydroxide. Another important parameter to introduce in the simulation is the presence of solid precipitates in the cavity. These solid phases, observed experimentally, act as a diffusion barrier, limiting the transport of H^+ ion outside of the cavity, but have also a chemical effect by buffering the pH in the cavity. This buffering effect is most probably at the origin of the higher pH observed in a quasi-steady state for a galvanized steel sheet in contact with a confined electrolyte, resulting from the precipitation of zinc corrosion products.

4. CONCLUSION

The pH evolution over steel surfaces in confined conditions was compared with that calculated using a two-dimensional transport-reaction model only in the case of a confined iron surface. The lower pH obtained experimentally was attributed to the limitation of the modelling approach, more especially concerning the presence of carbonate species (CO_2) and solid phases precipitation inside the cavity. Nevertheless, to be able to simulate the long term processes of corrosion perforation, the models have to be more complex to integrate the role of the corrosion products and the effect of CO_2 which is of importance as mentioned in recent works [17].

Acknowledgements. A. Q. Vu would like to thank Ho Chi Minh City University of Technology for the financial support of his project T-CNVL-2017-11.

REFERENCES

1. Vu A. Q., Vuillemin B., Oltra R., Allély C. – Microelectrode: An insitu measurement of the pH evolution for a laboratory test on a bare metallic surface, International Symposium on Materials Science and Engineering, 2017, Ho Chi Minh City – Viet Nam, ISBN: 978-604-63-2433-1.
2. Hoang Cuong – Design and simulation of the structure of a smart ink injector, Batchelor Thesis, University of Technology, Department of Electronic Engineering, 2012, (in Vietnamese).
3. Le Minh Thanh, Pham Hong Phong, Le Quoc Hung – Simulation of the declination of dissolved oxygen concentration along the lake depth, Proceedings of the annual scientific conference, 2014, ISBN: 978-604-82-1388-6 (in Vietnamese).
4. Ebrahimi Khabbazi A., Richards A. J., Hoorfar M. – Numerical study of the effect of the channel and electrode geometry on the performance of microfluidic fuel cells, Journal of Power Source **195** (2010) 8141-8151.

5. Zhanyu Sun, Agafonov V., Egorov E. – The influence of the boundary condition on anodes for solution of convection-diffusion equation with the application to a four-electrode electrochemical cell, Journal of Electroanalytical Chemistry **661** (2011) 157-161.
6. Francisco J. Almazán-Ruiz, Francisco V. Caballeroa, Martín R. Cruz-Díaz, Eligio P. Rivero, Ignacio González – Scale-up of rotating cylinder electrode electrochemical reactor for Cu(II) recovery: Experimental and simulation study in turbulence regimen, Electrochimica Acta **77** (2012) 262-271.
7. Matteo Scaramuzza, Alberto Ferrario, Elisabetta Pasqualotto, Alessandro DeToni – Development of an electrode/electrolyte interface model based on pseudo-distributed elements combining COMSOL, MATLAB and HSPICE, Procedia Chemistry **6** (2012) 69-78.
8. Eligio P. Rivero, Fernando F. Rivera, Martín R. Cruz-Díaz, Elvia Mayen, Ignacio González – Numerical simulation of mass transport in a filter press type electrochemical reactor FM01-LC: Comparison of predicted and experimental mass transfer coefficient, Chemical Engineering Research and Design **90** (2012) 1969-1978.
9. Edmund J. F. Dickinson, Henrik Ekstrom, Ed Fontes – COMSOL Multiphysics: Finite element software for electrochemical analysis. A mini-review, Electrochemistry Communications **40** (2014) 71-74.
10. Piyushkumar B. Tailor, Amit Agrawal, Suhas S. Joshi – Numerical modeling of passive layer formation and stabilization in electrochemical polishing process, Journal of Manufacturing Processes **18** (2015) 107-116.
11. Abishek Kamaraj, Spenser Lewis, Murali Sundaram – Numerical Study of Localized Electrochemical Deposition for Micro Electrochemical Additive Manufacturing, Procedia CIRP (Conference on Electro Physical and Chemical Machining) **42** (2016) 788-792.
12. Thébault F. – Influence des éléments d'addition dans les nouveaux procédés de revêtements sur les mécanismes de protection des aciers zingués, Doctorat Chimie Physique Dijon (Université de Bourgogne), 2008.
13. Bockris J. O'M., Khan S. U. M. – Surface Electrochemistry: a molecular level approach, Plenum Press, New York (1993) 335.
14. Weiss R. F. – Solubility of nitrogen, oxygen and argon in water and sea water, Deep Sea Res. **17** (1970) 721.
15. Lide D. R. – CRC Handbook of Chemistry and Physics 85th edition, CRC Press, Boca Raton (2005).
16. Toshima S., Nishijima M. – Kinetic study of oxygen reduction at a dropping mercury electrode, Denki Kagaku **36** (1968) 206.
17. Volovitch P., Allely C., Ogle K. – Understanding corrosion via corrosion product characterization: I. Case study of the role of Mg alloying in Zn–Mg coating on steel, Corros. Sci. **51** (2009) 1251–1262.